Oxygen Electrocatalysis on Mixed-Metal Oxides/Oxyhydroxides: From Fundamentals to Membrane Electrolyzer Technology

Raina A. Krivina, Yingqing Ou, Qiucheng Xu, Liam P. Twight, T. Nathan Stovall, and Shannon W. Boettcher*

Conspectus

Catalyzing the oxygen evolution reaction (OER) is important for key energy-storage technologies, particularly water electrolysis and photoelectrolysis for hydrogen fuel production. In neutral-to-alkaline conditions, first-row transition-metal oxides/(oxy)hydroxides are the fastest-known OER catalysts and have been the subject of intense study for the past decade. Critical to their high performance is the intentional or accidental addition of Fe to Ni/Co oxides that convert to layered (oxy)hydroxide structures during the OER. Unraveling the role Fe plays in the catalysis and the molecular identity of the true "active site" has proved challenging, however, due to the dynamics of the host structure and absorbed Fe sites, as well as the diversity of local structures in these disordered active phases.

In this *Account*, we highlight our work to understand the role of Fe in Ni/Co (oxy)hydroxide OER catalysts. We first discuss how we characterize the intrinsic activity of the first-row transition-metal (oxy)hydroxide catalysts as thin films by accounting for the contributions of the catalyst-layer thickness (mass loading) and electrical conductivity, as well as the underlying substrate's chemical interactions with the catalyst and the

presence of Fe species in the electrolyte. We show how Fe-doped Ni/Co (oxy)hydroxides restructure during catalysis, absorb/desorb Fe, and in some cases degrade or regenerate their activity during electrochemical testing. We highlight the relevant techniques and procedures that allowed us to better understand the role of Fe in activating other first-row transition metals for OER. We find several modes of Fe incorporation in Ni/Co (oxy)hydroxides and show how those modes correlate with activity and durability. We also discuss how this understanding informs the incorporation of earth-abundant transition-metal OER catalysts in anion-exchange-membrane water electrolyzers (AEMWE) that provide a locally basic anode environment but run on pure water and have advantages over the more-developed proton-exchange-membrane water electrolyzers (PEMWE) that use platinum-group-metal (PGM) catalysts. We outline the key issues of introducing Fe-doped Ni/Co (oxy)hydroxide catalysts at the anode of the AEMWE, such as the oxidative processes triggered by Fe species traveling through the polymer membrane, pH gradient effects on the catalyst stability, and possibly limited catalyst utilization in the compressed stack configuration. We also suggest possible mitigation strategies for these issues. Finally, we summarize remaining challenges including long-term stability of Fe-doped Ni/Co (oxy)hydroxides under OER conditions and the lack of accurate models of the dynamic active surface that hinder our understanding of, and thus ability to design, these catalysts.

1. Introduction

The ability of hydrogen (H_2) to serve as a medium between chemical and electrical energy makes it an attractive alternative to carbon-based fuels for powering transportation of people and goods, heating buildings, producing fertilizers, refining metals, and making

electricity with fuel cells.[1-2] Today most hydrogen is produced by steam-reforming of fossil fuels.[1] An alternative is water electrolysis. Water splitting involves two half-reactions: the oxygen-evolution reaction at the anode (OER; in base: $4OH^- \rightarrow 2H_2O + 4e^- + O_2$, in acid: $2H_2O \rightarrow 4H^+ + O_2 + 4e^-$) and hydrogen-evolution reaction at the cathode (HER; in base: $2H_2O + 2e^- \rightarrow H_2 + 2OH^-$, in acid: $2H^+ + 2e^- \rightarrow H_2$). Driving the OER results in a large overpotential (excess energy beyond the thermodynamic requirement) that decreases the efficiency of electrolyzers. Electrocatalysts capable of lowering the overpotential have been under investigation for nearly a century.

The oldest electrolyzer technology is alkaline water electrolysis (AWE). AWE is typically operated at ~ 80 °C in a concentrated basic liquid electrolyte (KOH or NaOH). Although the current densities are typically < 500 $mA \cdot cm^{-2}$, the low materials cost from the inexpensive (steel) cell components and non-PGM catalysts leads to a relatively low overall cost for hydrogen.[1] A newer technology, PEMWE, replaces liquid electrolyte with a solid, locally acidic, ionomer membrane.[3] Pure water is fed to a compressed stack allowing operation at > 2 $A \cdot cm^{-2}$ and yielding high-purity output hydrogen.[1, 3] The solid-polymer electrolyte reduces cross-over of hydrogen and oxygen gas, allowing thinner electrolytes with lower resistive losses and the direct electrochemical compression of the output hydrogen.[3] The acidic membrane, however, requires the use of PGM catalysts and expensive stack materials (e.g. Ti) because non-PGM catalysts corrode and dissolve.

AEMWE, in principle, can combine the advantages of AWE and PEMWE. The system uses the same compressed stack design as PEMWE but replaces the acidic membrane with a basic one enabling the use of non-PGM catalysts and cheaper stack materials.[1, 4] AEMWE is, however, at its early stage and has challenges to overcome before

it can compete in efficiency and durability with PEMWE. The design of active and stable OER and HER catalysts is imperative for the development and commercialization of AEMWE systems.

Iron-containing Ni and Co-based catalysts have superior OER performance in base and AWE compared to other catalysts including PGMs.[5-7] The origin of their high performance has been subject to much discussion. Friebel *et al*. reported Fe^{3+} as an active site in $Ni_{1-x}Fe_xOOH$ using a combination of *operando* X-ray absorption spectroscopy (XAS) and DFT calculations.[8] Gorlin *et al*. found that for $Ni_{1-x}Fe_xOOH$ with $x > 0.09$, Ni remains largely in +2 oxidation state during OER.[9] In contrast, Li *et al*. proposed that Fe^{3+} promotes the formation of Ni^{4+} that is responsible for the enhanced OER activity.[10] Smith *et al*. studied $Fe_{100-y}Co_yO_x$ and observed Co oxidation under OER conditions.[11] Gong *et al.* concluded that under-coordinated Fe^{3+} was an active site, despite Fe not being oxidized.[12] Hunter found evidence for Fe^{6+} and ferrate-like species in non-aqueous conditions and assigned these as the active sites in OER.[13] Chen *et al*. found Fe^{4+} under active conditions with Mossbauer spectroscopy, but demonstrated that this species persisted after the applied potential was removed.[14] The Fe cation sites are also dynamic; dissolving and redepositing depending on the concentration of solution Fe^{3+}.[15]

Understanding of the mechanism of OER in basic conditions and the identity of active sites is important for designing better catalysts for both AWE and AEMWE. Additionally, the effects of Fe adsorption/desorption, catalyst restructuring, and its electrical conductivity should be accounted for when incorporating $Ni(Co)_{1-x}Fe_xOOH$ into traditional AWE or membrane-electrode-assembly (MEA) systems.

Here we describe our efforts to identify and understand the active sites in Fe-doped Ni and Co (oxy)hydroxides. We aim to understand the mechanisms of Fe incorporation into the catalysts, the role played by Fe during OER, and how this understanding influences design principles for OER catalysts in electrolyzer technologies. Finally, we discuss research directions related to OER catalysts and electrolyzers relevant for high-performance non-PGM AEMWE.

2. Intrinsic Activity Trends for Metal (Oxy)Hydroxides

The use of thick catalyst layers and poorly-defined active surface areas, as well as differences in electrical conductivity and local surface structure, has historically complicated the direct comparisons of intrinsic OER activity.[6, 8] A better comparison can be made if the catalysts are prepared as thin films (2-3 nm) supported on conductive supports that minimize ohmic and mass-transfer overpotentials and the amount of inactive (bulk) catalyst.[16] This thin-film configuration also allows *in-situ* mass monitoring using a quartz crystal microbalance (QCM) and calculation of lower-limit turnover frequencies (TOF, the number of O_2 molecules evolved per metal active site per second) based on the total number of metal cations. The use of TOFs is a good metric for the comparison of intrinsic catalytic activity as long as the assumptions underlying the calculation are made clear. In alkaline media, for example, IrO_x is ~10-fold less active than $Ni_{0.9}Fe_{0.1}O_x$ (TOFs = 0.009 ± 0.005 s^{-1} and 0.21 ± 0.03 s^{-1} at η = 300 mV, respectively).[16] We compared the activities of many first-row transition metal oxides (NiO_x, CoO_x, $Ni_yCo_{1-y}O_x$, $Ni_{0.9}Fe_{0.1}O_x$, IrO_x, MnO_x, and FeO_x). We also analyzed if synergetic effects existed with two or more different metals. In the case of Co and Ni, we observed no synergy, in contradiction with

previous trends reported.[17-18] Addition of Fe to Co or Ni improved the performance to different degrees suggesting different interactions of Fe with the matrices.[16, 18] X-ray photoelectron spectroscopy (XPS) showed the catalysts were converted into (oxy)hydroxide phases during operation in agreement with thermodynamics-based Pourbaix diagrams.[16, 19] CoO_xH_y and NiO_xH_y both form layered structures with octahedrally coordinated metal cations and small ordered domain sizes where the individual layers are noncovalently bonded and intercalated with ions and water.[19-20]

The electrical conductivity of the catalyst phases is important in designing high-performance electrodes. For (oxy)hydroxides, the oxidation and protonation state of the material depends on applied potential, and therefore the conductivity is different than that measured from pressed catalyst-powder pellets. We measured thin-film conductivity as a

function of applied potential using microfabricated interdigitated array (IDA) electrodes.[19, 21-22] We discovered that the conductivity varied with composition and applied potential. CoO_xH_y and NiO_xH_y were insulating when the cations were +2, and conductive when oxidized to nominally +3 or +4; a conversion that happens under OER conditions and that is (usually) reversible. The redox behavior of CoO_xH_y and NiO_xH_y provides another mechanism to measure the number of electrochemically accessible metal cations which can be done by integrating the pre-OER redox feature visible in the voltammetry.[23] It is important to note, however, that exactly which of these electrochemically accessible metal sites are catalytic site remains an open question.[24-27]

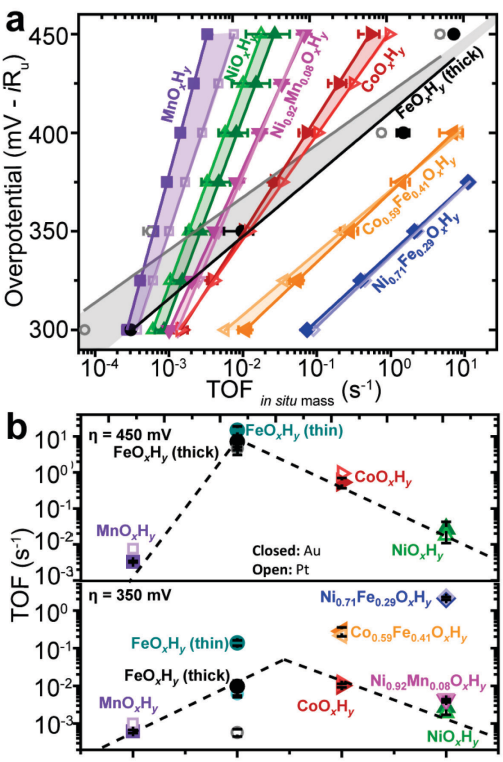

Figure 1. (a) Steady-state activity trends as a function of potential for first-row transition-metal (oxy)hydroxides on Au (solid) and Pt (open) quartz-crystal-microbalance electrodes. The TOFs reported are based on the total mass measured with the QCM assuming every metal cation is a possible active site. (b) The data plotted at $\eta = 450$ mV (top) and at $\eta = 350$ mV (bottom). Compositions in (b) are ordered based on atomic number of the host/primary cation. Lines and shading guide the eye. All the films had a loading of 8 to 12 μg·cm^{-2}, except for the thin FeO_xH_y which was 0.5−1.0 μg·cm^{-2}. Adapted from ref 30 with permission. Copyright 2015 American Chemical Society.

XPS analysis of thin-film CoO_xH_y and NiO_xH_y catalysts revealed Fe impurities absorbed from the electrolyte even without intentional addition of Fe salts.[16, 19, 21] To observe the intrinsic activity, Fe impurities had to be removed. We produced Fe-free KOH by absorbing Fe species with $Ni(OH)_2$ and $Co(OH)_2$.[19] We note that these Fe-free electrolytes do contain residual $Co(OH)_2$ or $Ni(OH)_2$ that can be removed by filtration with

a 0.1 μm polyethersulfone filter. The catalysts tested in Fe-free KOH did not show any traces of Fe incorporation by XPS.[19] We then reported the first intrinsic activity trend of first-row transition metals with rigorous exclusion of Fe-impurities. We accounted for the influence of the film thickness, conductivity, and underlying substrate interactions (**Figure 1**).[28-30] We discovered that, in the absence of Fe, NiO_xH_y was a terrible OER catalyst – three-orders-of-magnitude less active than $Ni(Fe)O_xH_y$.[19] CoO_xH_y shows higher activity than NiO_xH_y in the absence of Fe, but when Fe is added, $Ni(Fe)O_xH_y$ has a higher TOF than $Co(Fe)O_xH_y$ at all overpotentials.[21] The activity of FeO_xH_y was found to be strongly dependent on the film thickness and the support (see below).[28, 30-31] At this point, we proposed that Fe was an *essential component* of the active site in *all* the first-row transition-metal catalysts in alkaline conditions (with reasonably high activity) whether incorporated intentionally or from the electrolyte impurities.[28]

3. Understanding Fe-based Active Sites

To better understand how Fe-based OER catalysts function, we studied pure FeO_xH_y.[28] To do this, the instability of FeO_xH_y under alkaline OER conditions and its low electrical conductivity had to be addressed. FeO_xH_y films were prepared by three methods – electrodeposition,[19, 32] thermal decomposition of a spin-cast metal-nitrate films,[16] and thermal evaporation of Fe metal – and were probed by XPS after annealing in air and immersion in 1 M KOH.[30] Fe was oxidized to nominally FeOOH under these conditions regardless of preparation method. Using electrodeposited FeO_xH_y films, the dependence of OER activity on the substrate type (Au and Pt) and film thickness was investigated (correcting for dissolution via QCM mass measurements). At η = 350 mV, the OER current

was insensitive to mass loading, but depended on the substrate identity with FeO_xH_y on Au much more active than on Pt (likely due to interaction of Fe and Au oxides under OER conditions).[31, 33] At η = 450 mV, the OER current was proportional to FeO_xH_y loading up to ~3 $\mu g \cdot cm^{-2}$ before increasing slower between 3 and 7.5 $\mu g \cdot cm^{-2}$ and remaining constant after 7.5 $\mu g \cdot cm^{-2}$. We concluded that only a thin layer of FeO_xH_y nearest to the electrode surface is active at η = 350 mV due to the low electrical conductivity of FeO_xH_y. At η = 450 mV, the thickness of the active layer increases because the electrical conductivity increases as the Fe accesses higher oxidation states.[30]

The comparison of the intrinsic activity of $Ni(Fe)O_xH_y$, $Co(Fe)O_xH_y$, and FeOOH was made by calculating TOF per "electrochemically active" Fe site (TOF_{Fe}) at η = 350 mV and 450 mV. To account for limited conductivity, we approximated the amount of "active" FeO_xH_y as that within a loading range such that < 1 mV of Ohmic drop occurs at 1 $mA \cdot cm^{-2}$ (0.1 $\mu g \cdot cm^{-2}$ at 350 mV and 5 $\mu g \cdot cm^{-2}$ at 450 mV). It was observed that at η = 350 mV and 450 mV, $Ni_{0.75}Fe_{0.25}OOH$ had a higher TOF_{Fe} than $Co_{0.54}Fe_{0.46}OOH$ and FeO_xH_y /Au. This data suggested that the "host", and therefore local chemical environment of Fe, enhances the OER activity.[28]

We investigated how Fe was involved in OER using *operando* XAS. For this we studied $Co(Fe)O_xH_y$, which shares key features with $Ni(Fe)O_xH_y$. The OER activity of $Co(Fe)O_xH_y$ increases 100-fold with 40%-60% co-deposited Fe relative to Fe-free CoO_xH_y. Voltammetric analysis shows an anodic shift in the $Co^{2+/3+}$ redox wave with increasing Fe content suggesting strong electronic coupling between Co and Fe.[21] The nominally $Co^{2+/3+}$ wave is, however, more negative than the nominally $Ni^{2+/3+}$ wave, even in the presence of large amounts of Fe. This is important, because it allowed us to resolve the local structure

and oxidation states at both Fe and Co sites by XAS at potentials more positive of the Co wave (i.e. when the catalyst is in the relevant oxidized "active-state" but not yet evolving oxygen) and compare to more-positive potentials where substantial OER current is passing. Compared to previous studies,[8, 13-14] our work was important because we engineered porous catalyst structures as thin films where essentially all the Co and Fe sites were exposed to electrolyte.[7] The porous structure was achieved by electrodeposition/precipitation from a precursor salt solution via the cathodic reduction of NO_3^- that raises the pH at the electrode surface.[7] The XAS thus reported on changes to surface-active Co and Fe sites without large background signal from sites buried and not accessible to the electrolyte. In $Co(Fe)O_xH_y$, we found a 6% decrease in the Fe-O bond length and a small absorption-edge shift at OER potentials indicating partial oxidation of Fe relative to

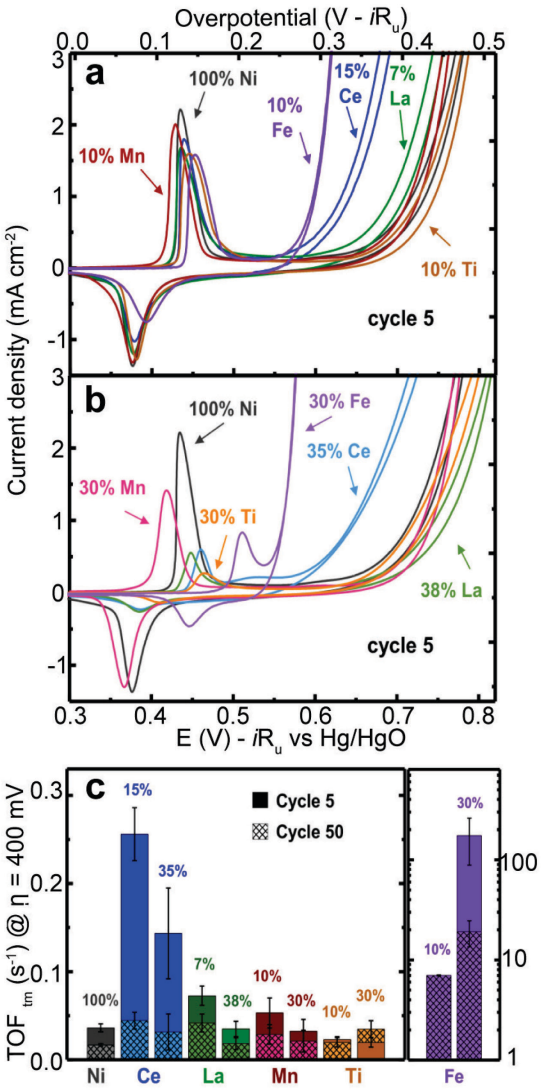

Figure 1. Cyclic voltammetry (cycle 5) of spin-cast $Ni_{1-z}M_zO_xH_y$ films, where M is the metal cation (Ce, La, Mn, Ti and Fe), at approximately (a) $z \approx 0.1$ and (b) $z \approx 0.3$ in Fe-free 1 M KOH at 20 $mV \cdot s^{-1}$. (c) OER TOF of spin-cast films at 400 mV overpotential at cycle 5 (solid) and cycle 50 (pattern) in Fe-free 1.0 M KOH from voltammetry data collected at 20 $mV \cdot s^{-1}$. TOF_{tm} are calculated assuming all metal cations are active (and thus are lower limits); the OER current is taken as the average of the forward and reverse scans. Adapted from ref 36 with permission. Copyright 2016 American Chemical Society.

the pre-OER resting state (likely 3+).[7] Oxidation of Co was only observed in Fe-free CoO_xH_y consistent with Fe being a key species at the active site involved in stabilizing OER intermediates.[7]

Although NiO_xH_y is intrinsically less active than CoO_xH_y, $Ni(Fe)O_xH_y$ is more-active than $Co(Fe)O_xH_y$. In NiO_xH_y a lower OER onset potential upon Fe incorporation is accompanied by an positive shift of the $Ni^{2+/3+}$ wave.[19] Others correlated the increased OER activity to this shift[34-35] and hypothesized that charge transfer from Ni^{2+} to the Lewis-acidic Fe^{3+} makes the Ni site more oxidizing and facilitates the oxidation of water into O_2.

We doped NiO_xH_y with Fe, Ti, Mn, La, and Ce cations and studied the correlation between the $Ni^{2+/3+}$ potential and OER activity.[36] Solution spin-casting and electrodeposition were used to prepare films with well-mixed cations and similar mass loading and morphology (**Figure 2a-b**).[36] Ce was the only cation besides Fe which enhanced the activity of NiO_xH_y (**Figure 2c**). During the initial voltammetry in rigorously "Fe-free" KOH solution, $Ni_{0.85}Ce_{0.15}O_xH_y$ and $Ni_{0.65}Ce_{0.35}O_xH_y$ exhibited activities ~ 8 and 4 times higher than pure NiO_xH_y, respectively. The increased activity of Ce-incorporated films declined during cycling. The O 1s XPS spectra of $Ni(Ce)O_xH_y$ collected before and after extended cycling showed a change from a metal hydroxide to oxide. We interpreted this as phase-segregated cerium oxides forming that eliminated the more-active Ni-O(H)-Ce motifs.

The incorporation of Ti, Mn, or La cations into NiO_xH_y did not improve activity.[36] Ti and La shifted the Ni redox wave positive, but the OER activity remained the same as in the pure NiO_xH_y. The lack of activity enhancement accompanying the shift in $Ni^{2+/3+}$ redox potential indicates that there is no strong relationship between the two. In retrospect,

this is perhaps not surprising as after the oxidation of the Ni/Co, the films are conductive with relatively delocalized electronic structures and additional applied potential will increase the oxidative driving force regardless of the initial $Ni^{2+/3+}$ wave position.[37-38] The unique role of Fe in enhancing the OER activity also supports the idea that Fe serves a critical role – likely bonding to intermediates – as a part of the "active site".

4. Modes of Fe Incorporation in Ni/Co (Oxy)Hydroxides

We explored three ways of incorporating Fe into Ni/Co (oxy)hydroxides: co-deposition, adsorption from electrolyte impurities, and adsorption from Fe-spiked electrolyte. We found that the activity enhancement relative to how much Fe is incorporated depended on the incorporation method and that some Fe sites appear more active than others.[39] We cycled a freshly electrodeposited NiO_xH_y film in Fe-spiked KOH (1 mM $Fe(NO_3)_3$). After the initial cycles, a dramatic increase in activity was observed, as evidenced by the > 100 mV decrease in onset potential (**Figure 3a**). Meanwhile, the Ni redox peak potential and

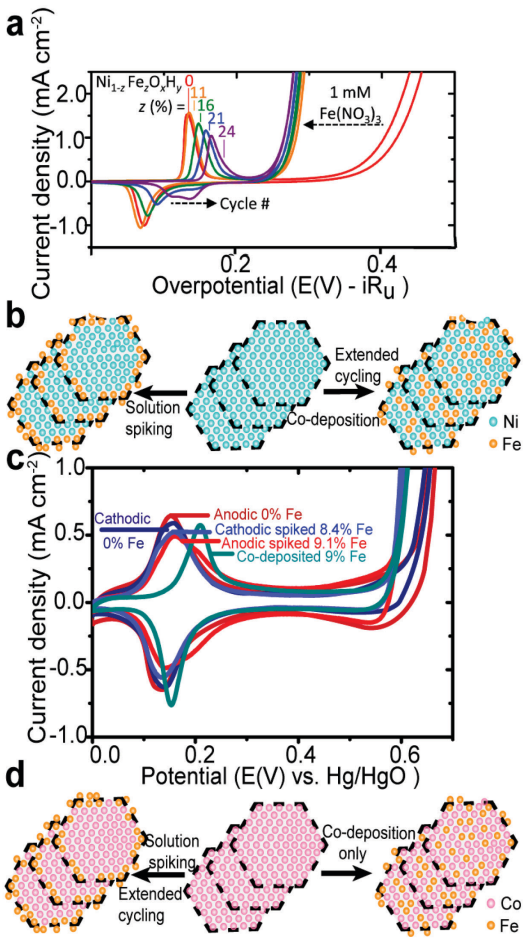

Figure 3. (a) CVs showing spiking 1 mM Fe^{3+} leads to 130-150 mV decrease in overpotential for NiO_xH_y in the first 2 cycles with much smaller decrease over the next 98 cycles. 24% Fe is incorporated into NiOOH compared to only ~9% in CoO_xH_y after 50 cycles (c). The extended cycling studies suggest that Fe permeates into the bulk of NiO_xH_y (b) but only accesses the surface of CoO_xH_y (d). Adapted from ref 39 and 15.

average e^- per Ni in the redox wave, was largely unchanged.[39] After 100 cycles, the anodic peak potential ($E_{p,a}$) of NiO_xH_y shifted positive by ~30 mV. In contrast to the change in the $E_{p,a}$, the OER activity was only marginally improved after 100 cycles, even as Fe was incorporated up to 24%. This suggested that Fe species might initially be absorbed on the edge/defect sites where they drive fast water oxidation while having little influence on the Ni redox features whereas further Fe incorporation by cycling leads to (inactive) Fe sitting on "internal" sites within the 2D (oxy)hydroxide structure.

We compared the results to a co-electrodeposited $Ni(Fe)O_xH_y$ film and found for similar Fe content the co-deposited $Ni(Fe)O_xH_y$ shows a more-prominent positive shift of the Ni redox peak. We hypothesize that co-deposited $Ni(Fe)O_xH_y$ have Fe homogeneously distributed throughout the structure that strongly interacts with Ni, substantially affecting the average Ni redox properties. The fact that the OER activity of $Ni(Fe)O_xH_y$ appears not to depend on the "bulk" electronic structure or the $Ni^{2+/3+}$ redox peak potential suggests that it is the surface-bound, under-coordinated Fe sites that are responsible for the high OER activity. Chen *et al*. also proposed that due to the disordered structure of the deposited $Ni(Fe)O_xH_y$ there exists edge/defect sites which host Fe species and these Ni-O-Fe motifs are responsible for efficient water oxidation.[14] This proposal was based on the observation of long-lived Fe^{4+} sites in Mössbauer experiments that are evidently not highly OER active.

Similar to $Ni(Fe)O_xH_y$, incorporation of Fe into CoO_xH_y via cycling in Fe-spiked KOH results in enhanced OER activity.[15] However, Fe appears difficult to incorporate into the "bulk" structure of CoO_xH_y, as evidenced by the almost unchanged $E_{p,a}$ after extended cycling (**Figure 3b**). This result can be explained by the stronger Co-O, compared Ni-O, bond.[40] After cycling CoO_xH_y in Fe-spiked KOH, we transferred the $Co(Fe)O_xH_y$ to Fe-

free KOH. With further cycling, a fast deactivation process was observed. Post-mortem XPS characterization showed a 60% decrease in the Fe content.[15] In comparison, co-deposited Co(Fe)O_xH_y showed little activity loss when cycled in Fe-free KOH and XPS showed only ~10% Fe loss. These results suggest that dynamic Fe species are incorporated during cycling in Fe-spiked KOH. These Fe likely reside at surface edge/defect sites and thus easily dissolve in Fe-free electrolyte during OER when solution Fe is absent and hence cannot replenish the surface Fe sites. Fe in the co-deposited Co(Fe)O_xH_y film is distributed throughout the film which prevents its rapid loss in Fe-free KOH.

We further applied electrochemical atomic-force microscopy (EC-AFM) to study morphology dynamics during OER. We began with single-layer $Ni(OH)_2$ (SL-$Ni(OH)_2$) nanosheets synthesized hydrothermally and exfoliated.[41] In the absence of Fe, the SL-$Ni(OH)_2$ preserved its original hexagonal shape and smooth surface at the open-circuit voltage (OCV) in 0.1 M KOH (**Figure 4a**).[42] With an increase in potential to 1.41 V vs. RHE, which corresponds to the onset of Ni oxidation, the SL-$Ni(OH)_2$ roughened (**Figure 4b**). Further increases in potential lead to restructuring of the single nanosheets into nanoparticles (**Figure 4c, d**). The volume and surface area of the nanoparticles increased with cycling. Once the growth of the $Ni(OH)_2$ nanoparticles halted, we introduced 3 ppm of $Fe(NO_3)_3$ into the electrolyte (**Figure 4g**). The Fe spike caused a ~19% volume

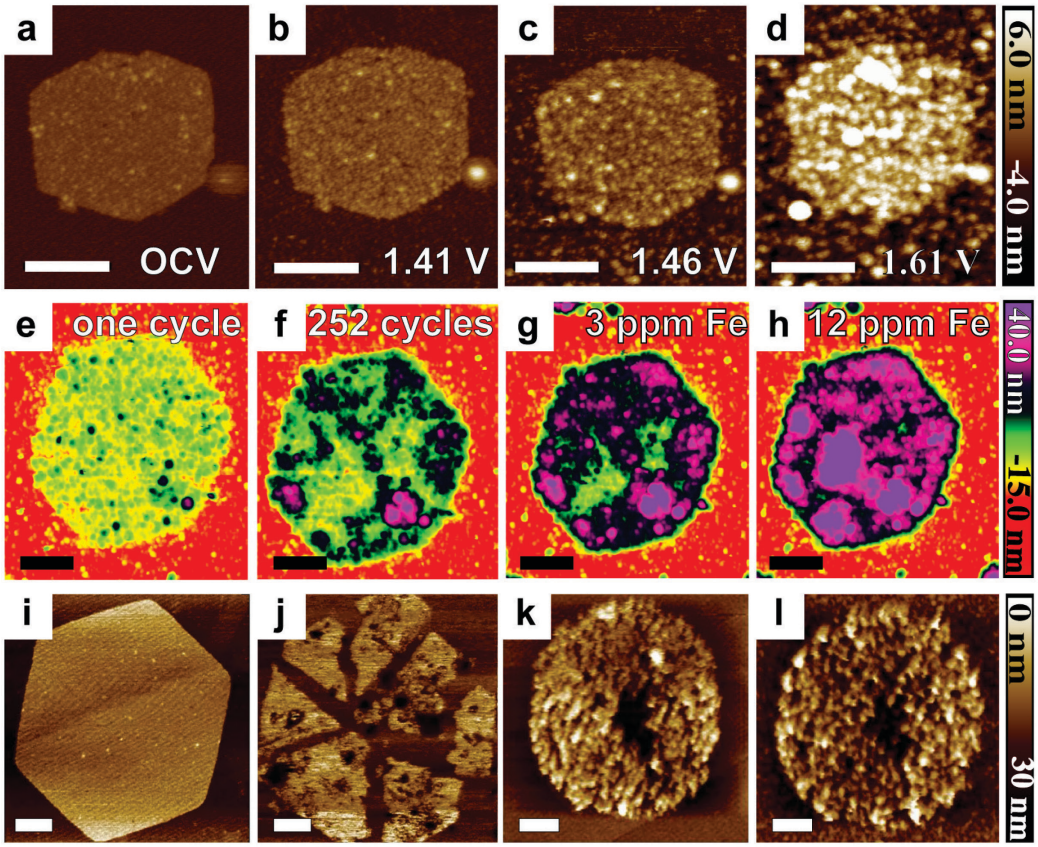

Figure 4. AFM images of SL-$Ni(OH)_2$ in Fe-free KOH (a) at the open-circuit voltage, and then after the chronopotentiometry measurement (for 500 s) at (b) 1.41 V vs RHE, (c) 1.46 V vs RHE, and (d) 1.61 V vs RHE (scale bars = 200 nm), (e) after one LSV in 0.1 M KOH, (f) after 252 CV cycles, and in the presence of (g) 3 ppm $Fe(NO_3)_2$ and (h) 12 ppm $Fe(NO_3)_2$ after three CV cycles (scale bars = 200 nm). AFM topographical images of $Ni_{0.8}Co_{0.2}O_xH_y$ nanosheets (i) at the beginning and (j) after 200 CV cycles between 1 and 1.7 V vs. RHE in 0.1 M KOH (scale bars = 100 nm). SL-$Co(OH)_2$ nanosheets images under identical conditions (k) at the beginning and (l) after the electrochemical testing. Adapted from ref 42 and 43.

expansion after three CVs and Fe was observed to deposit inhomogeneously. After Fe in KOH was increased to 12 ppm, segregated FeOOH appeared to deposit (**Figure 4h**). The restructuring of the $Ni(OH)_2$ nanoparticles during Fe incorporation might explain how Fe moves into the bulk during extended CV cycling. The morphology changes seem to be the result of a Ni dissolution/redeposition process.[42-43]

$Co(OH)_2$ nanosheets undergo less morphological changes under electrochemical conditions.[43] EC-AFM showed that Co-rich $Ni_{1-\delta}Co_\delta O_xH_y$ and CoO_xH_y initially had a porous morphology and the higher porosity was likely able to reduce the mechanical stress

that originated from redox (**Figure 4i-l**). As a result, Co-rich $Ni_{1-\delta}Co_{\delta}O_xH_y$ exhibited higher electrochemical and mechanical stability consistent with our hypothesis that Fe absorbed from the electrolyte is difficult to incorporate into the bulk of CoO_xH_y.[15, 43]

Markovic and coworkers used scanning tunneling microscopy (STM) and ICP-MS techniques combined with isotope labelling to investigate the dynamic stability of Fe sites in transition-metal (oxy)hydroxide clusters.[44] STM revealed that the cluster height of Ni (oxy)hydroxide on Pt(111) slightly increased when the electrode was immersed in Fe-spiked KOH solution, suggesting that Fe was adsorbed on the surface. The dynamic Fe exchange at the catalyst-electrolyte interface was monitored by isotopic labelling starting with ^{56}Fe on the electrode and ^{57}Fe in the electrolyte. ^{56}Fe dissolved during chronoamperometry, while ^{57}Fe in electrolyte deposited onto the electrode surface. The system eventually reaches a dissolution-redeposition steady state. During activity tests in Fe-spiked electrolyte, OER performance improved. When measured in Fe-free KOH, the OER performance degraded, consistent with our results above. The sum of these studies indicates that the high OER activity of Fe-MO_xH_y can only be maintained in the presence of Fe in the electrolyte, supporting the view that the dynamic Fe exchange underlies the stability/performance of these catalysts.

We further studied how more-complex compositions behave in an effort to increase intrinsic activity/stability as well as better understand mechanism. For example, others reported that mixed Ni-Co-Fe (oxy)hydroxides are more active than NiFe systems,[45-46] although explanations for the activity trends differed and the measurements were not performed in a way where reliable intrinsic activities could be confirmed. We considered several reasons why addition of Co might enhance activity of Ni(Fe)O_xH_y: 1) the onset

of CoO_xH_y electrical conductivity is at lower overpotentials so active sites might become electrochemically accessible at more negative potentials; 2) CoO_xH_y may uptake more Fe than NiO_xH_y before Fe phase segregates so addition of Co might allow formation of more Fe active sites, 3) the electronic interaction of Fe, Ni and Co might yield more-optimal intermediate binding energies. For some more-complex compositions, morphological changes can increase the active-Fe-site density due to leaching during OER, as likely observed for Cr-containing Ni-Fe (oxy)hydroxides or other compositions with base-soluble cations.[47-48]

We first evaluated the OER activity of $Ni(Co)O_xH_y$ with the rigorous exclusion of Fe impurities.[18] Generally a single redox wave was observed for the mixed-metal system that shifted negatively with increasing Co. This data suggests a strong electronic interaction between homogeneously mixed Ni and Co cations. The most-active binary composition was only two-fold more active compared to the parent compounds. We then examined the ternary $Ni(Co,Fe)O_xH_y$ and found that the best composition was only ~1.5 times more active than $Ni(Fe)O_xH_y$ on a per-metal-cation TOF basis.[18] The OER activity for pure and Fe-containing binary Ni/Co compounds does not correlate with the position or size of the redox waves which instead correlate with "bulk" composition of the system.

5. Towards Advanced Electrolysis: Ni and Co-based Catalysts with Dynamic Fe Sites in AEMWE

AEMWEs in principle allow for the use of earth-abundant OER catalysts over IrO_2 required for commercial PEMWE.[1, 49-50] While the AEM provides a locally basic

environment, the feed is often pure water and a detailed chemical understanding of the activity and durability of OER catalysts in these conditions is missing.

We compared the performance of first-row transition metal (oxy)hydroxide/oxide catalysts in three-electrode alkaline electrolytes and AEMWE in pure water.[49] The best OER catalyst in alkaline electrolyte, $NiFeO_xH_y$, performed poorly in AEMWE. However, we found a correlation between the electrical conductivity of the catalyst, measured *ex-situ*, and the performance of the electrolyzers (**Figure 5**). $NiCoO_x$, $NiCoO_x$:Fe, and $NiCoFeO_x$ with high intrinsic electronic conductivity show smaller cell voltages at 0.2 $A \cdot cm^{-2}$, better than IrO_x. $NiFeO_xH_y$ shows the lowest *ex-situ* conductivity (6×10^{-9} $S \cdot cm^{-1}$) and the highest cell voltage.[49] In the absence of the liquid electrolyte, we hypothesize that the bulk of $NiFeO_xH_y$ cannot convert to a conductive oxidized form which prevents high activity.

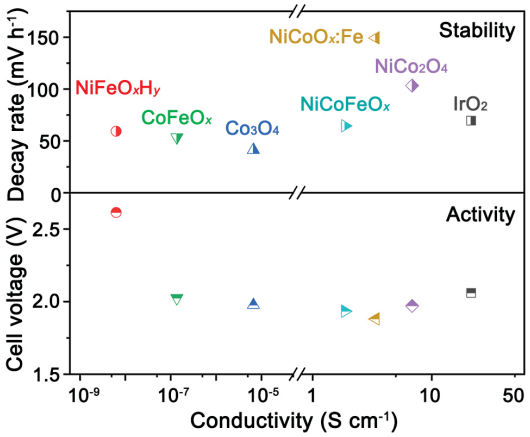

Figure 5. The electrical conductivity, activity, and degradation rate in pure-water AEMWE at 0.2 $A \cdot cm^{-2}$ of a series of the first-row transition metal (oxy)hydroxide/oxide catalyst powders. Adapted from ref 49.

Work in liquid electrolyte shows that absorbed Fe participates in a dissolution-redeposition equilibrium and is an essential component of the active site.[44] In a typical AEMWE system with pure-water feed, dissolved Fe would enter the neutral water flow where its solubility is higher than in alkaline electrolyte. This phenomenon might explain why the $NiCoO_x$:Fe (with Fe mainly adsorbed on the surface) degraded quicker than the

$NiCoFeO_x$ (prepared by co-precipitation of Ni, Co, and Fe) during our AEMWE stability test.

In three-electrode experiments a thin catalyst layer is deposited on conductive electrodes in 1.0 M KOH with rapid stirring to enhance mass transport. The KOH permeates the porous catalyst assembly in ways the solid ionomer cannot. Three-electrode conditions thus do not account for the bottlenecks of the MEA including catalyst utilization, mass-transport limitations (water and gas), and ionic (OH^-) and electrical conductivity. Thus, lab-scale results obtained via alkaline electrolyte cells can be more promising than those measured in an AEMWE.[51]

Kim *et al*. showed high performance for Ni-Fe-based nanofoam OER catalyst in pure water (2.7 $A \cdot cm^{-2}$ at 1.8 V, 85 °C) using a highly basic ammonium-enriched ionomer, but the performance decayed rapidly (1.3 $mV \cdot h^{-1}$ at 200 $mA \cdot cm^{-2}$ and 60 °C) which was attributed to oxidation of the ionomer but is also likely due to flushing of residual KOH from the system (**Figure 6 blue trace**).[50] Yan and co-workers demonstrated that by growing Fe_xNi_yOOH directly on a compressed Ni foam one avoids the use of Ti or stainless-steel gas diffusion layers (GDL) altogether, improves access to the active sites through the pores in the foam, and reduces the catalyst loss during operation in pure water (1020 $mA \cdot cm^{-2}$ at 1.8 V, 80 °C; 0.56 $mV \cdot h^{-1}$ for > 160 h at 200 $mA \cdot cm^{-2}$) (**Figure 6, red trace**).[52] Good initial AEMWE performance is evidently achievable with non-PGM catalysts in pure water, but stability remains a serious issue that can only be solved by understanding and controlling the ionomer and catalyst chemistry during OER.

We used a reference electrode with an AEMWE stack to measure the impedance and polarization responses of the anode and cathode separately.[53] This technique is valuable in pinpointing the source of performance loss, particularly when using impure water feeds.[2] We also developed easily adoptable procedures for MEA fabrication and a baseline for AEMWE performance in pure water with all commercial components (0.67 $mV \cdot h^{-1}$ after break-in at 500 $mA \cdot cm^{-2}$, 55 °C): PiperION PAP-TP-85 ionomer/membrane, steel GDL, and IrO_2 anode and Pt cathode (**Figure 6 orange trace**).[54] Soni *et al* further showed promising durability with a trimethylammonium-modified poly(fluorene-alttetrafluorophenylene)s membrane and ionomer **(Figure 6 green trace)**.[55]

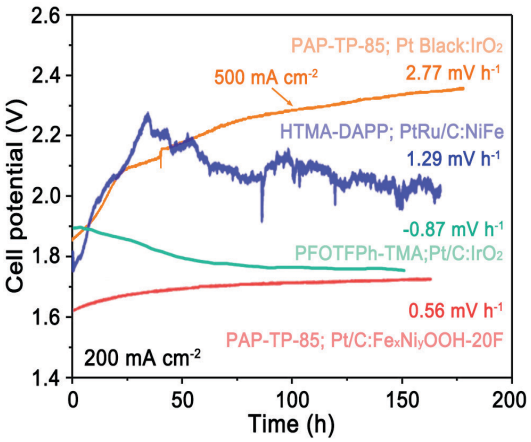

Figure 6. A summary of AEMWE performance in pure water at 200 $mA \cdot cm^{-2}$ (except orange trace, 500 $mA \cdot cm^{-2}$). Catalysts, membrane materials, and degradation rates are identified for each trace. Adapted from ref 50, 52, 54, and 55.

Possible effects of dynamic Fe sites on membrane stability. Most AEMWE tests use PGM catalysts or basic liquid electrolytes that minimize catalyst instability.[56-57] Substantial *in situ* and post-operation chemical analysis is usually lacking. Fe enhances the OER activity of Co and Ni-based catalysts when absorbed on the surface or substituting Ni or Co sites.[15, 44, 58] The maintenance of high activity is contingent upon sufficient Fe in the electrolyte[44, 58] such that the rate of Fe deposition equals that of dissolution.[44] The presence of Fe cations in the water feed will likely have detrimental effect on durability, for example due to Fenton processes with hydrogen peroxide.[2] Hydrogen peroxide can be formed by gas mixing in the stack.[3] Degradation can be avoided by preventing gas crossover which

requires more-selective AEMs. Fe cations travelling through the membrane from the anode will also deposit on the cathode causing HER activity loss or may accumulate in the membrane and precipitate. Post-operation chemical analysis of the membrane (EDX, XPS, NMR), catalyst structure at the anode and cathode (XRD, SEM, XPS), as well as *in situ* ICP-MS analysis of the outgoing water flow appears needed to detect catalyst leaching and redistribution.

One strategy to reduce Fe leaching may be to incorporate it within the catalysts bulk structure. However, the preferential leaching of Fe compared to Ni in highly basic conditions and elevated temperatures in such devices will have to be addressed.[59-60] Improvement of stability can be achieved through novel synthetic methods and taking advantage of the catalyst/support interactions.[61] The MEA configuration, though, might help to prevent the loss of dissolved species and favor their redeposition at the anode while a more-selective AEM will slow the crossover of the those species to the cathode.[2] At the cathode, adjusting the water flow and current densities along with selecting an HER catalyst with a crystal structure different from the precipitating/depositing species may minimize deactivation.[2]

Catalyst utilization. Unlike catalyst immersed in KOH, the catalyst embedded in an ionomer pressed against the solid-ionomer membrane has a limited supply of OH^- that must travel through the membrane and ionomer/catalyst network.[49, 51] The catalyst powders are usually spray-coated on a porous transport layer (PTL). Good electrical contact to the PTL is crucial for Ni and Co-based catalysts that have lower intrinsic electrical conductivity than IrO_2. Hegge *et al*. demonstrated that utilization can be improved by maximizing the catalyst porosity and electrical contact using nanofibers.[62] The phase

transformation and surface reconstructions observed during OER for Ni-based transition-metal (oxy)hydroxides also present challenges. In a MEA, the ionomer and the membrane are responsible for carrying OH^-. Dynamically changing catalyst/membrane and catalyst/ionomer interfaces might cause interruptions in the OH^- transport chain, which, along with limited electrical conductivity in poorly integrated catalyst/PTL configurations, might result in high ohmic losses.

pH changes at the anode/membrane interface. Operating AEMWE with a pure water feed at high current densities will affect the pH at the anode. Holdcroft *et al.* visualized the transport of OH^- through an AEM from cathode to anode during electrolysis demonstrating that the interface between the anode and the membrane remains less basic than the rest of the membrane due to the fast consumption of OH^-.[4] Non-PGM transition-metal oxides dissolve faster at lower pH which presents a durability challenge for PGM-free AEMWE.[3] Another source of acidification at the anode is ionomer oxidation. Yu Seung Kim *et al.* studied the acidification of phenyl-containing AEMs by phenol formation and showed how it leads to performance loss in AEMFCs.[63] Membrane acidification might be decreased by replacing the phenyl groups in the backbone with more oxidatively stable components and minimizing their adsorption onto the catalyst surface[50] by tuning the phenyl adsorption energy.[63]

It is still, however, not clear what the pH is at the catalyst surface during operating AEMWE in pure water or with a supporting electrolyte. Means of measuring the pH at these nanoscale interfaces would be useful as would non-PGM OER catalysts with wider pH stability. Co and Ni-based catalysts corrode and dissolve at acidic pH,[64] although Co

oxides appear more pH-stable than Ni oxides. Fe, Ni, and Co might be paired with more-acid-stable elements like Sb or Ti to improve durabilty.[65]

6. Conclusion and Outlook

Despite decades of work, there remains substantial need to further understand and control the OER reaction in alkaline conditions – particularly in the context of the dynamic Fe sites in AWE and AEMWE systems. Based on our work, and that of many others around the world, we have learned the following lessons: 1) crystalline metal oxides that are capable of driving OER at relatively low overpotential are structurally dynamic in alkaline, oxidizing conditions, favoring hydrated disordered (oxy)hydroxide phases during operation, 2) minimizing electrical-conductivity and mass-transport limitations are essential for fundamental activity measurements and for engineering high performance in practical electrodes, 3) dynamic adsorption or incorporation of Fe is central for the highest-activity catalysts and Fe is a key component of the OER active site and very likely directly bonding with intermediates, 4) bulk materials properties, either of oxides themselves or even of the active (oxy)hydroxide phases (such as the Co/Ni redox potential, e_g orbital filling, covalency, etc.), are not simply correlated with the OER activity. Local electronic and structural descriptors are probably needed to rationalize OER activity.

We suspect these lessons are universally applicable to OER catalysts in alkaline conditions. It is established that phosphide- and sulfide-based OER catalysts serve only as precursors to the (oxy)hydroxide phases discussed above[66] and we have not been able to observe high catalytic OER activity from *any non-precious-metal material* in the rigorous absence of Fe. Further, Binninger and coworkers argue that all metal oxides are unstable

under OER conditions.[67] This appears particularly true for high-activity perovskite oxides, such as $Ba_{0.5}Sr_{0.5}Co_{0.8}Fe_{0.2}O_3$ (BSCF) which was identified as a material with high OER activity on the basis of molecular orbital principles[68] (assuming retention of the as-prepared crystalline morphology during OER). Later, it was discovered that surface reconstruction and cation leaching leads to Co(Fe)OOH shells.[69-70] Epitaxial [001]-oriented $LaNiO_3$ single crystals rearrange to (oxy)hydroxides when Ni-terminated (but not when La-terminated and largely OER-inactive).[71] $La_{1-x}Sr_xCoO_3$ formed a thin CoOOH layer that absorbs Fe which was most pronounced for the higher Sr-substituted species.[72] The chemical tunability, high activity, and structural dynamicity of perovskite oxides makes them a rich system for further study of surface-absorbed Fe. All these dynamic processes should be accounted for in AWE and AEMWE systems in order to design for optimal performance and durability. Much work remains.

Notes

The authors declare no competing financial interest.

Author Information

Corresponding Author

Shannon W. Boettcher – Department of Chemistry and Biochemistry, University of Oregon, Eugene, 97403, USA. http://orcid.org/0000-0001-8971-9123

Email: swb@uoregon.edu

Authors

Raina A. Krivina - Department of Chemistry and Biochemistry and the Oregon Center for Electrochemistry, University of Oregon, Eugene, 97403, USA. http://orcid.org/0000-0002-4582-3743

Yingqing Ou – Chongqing University, China. http://orcid.org/0000-0002-0121-2684

Qiucheng Xu – East China University of Science and Technology, Shanghai, China. https://orcid.org/0000-0002-2771-9643

Liam P. Twight – Department of Chemistry and Biochemistry, University of Oregon, Eugene, 97403, USA. http://orcid.org/0000-0002-3430-4497

T. Nathan Stovall - Department of Chemistry and Biochemistry, University of Oregon, Eugene, 97403, USA. http://orcid.org/0000-0001-5808-5877

Biographies

Shannon W. Boettcher

Shannon W. Boettcher is a Professor in the Department of Chemistry and Biochemistry at the University of Oregon and the Founding Director of the Oregon Center for Electrochemistry. His research interests center on understanding and developing inorganic materials for energy conversion and storage.

Raina A. Krivina

Raina A. Krivina received her B.S. in chemistry at the Richard Stockton University of New Jersey. She is currently a fourth-year Ph.D. candidate at the University of Oregon.

Her research focuses on understanding degradation pathways in AEMWE, designing new catalyst materials for PEMWE, and nanomaterials synthesis.

Yingqing Ou

Yingqing Ou received his B.S. in chemistry from Sichuan University in 2009. He is a Ph.D. candidate in chemistry and chemical engineering at the Chongqing University, China. He is currently a visiting scholar at the University of Oregon. His research interests focus on the synthesis of nanomaterials and their applications in energy conversion.

Qiucheng Xu

Qiucheng Xu is a joint Ph.D. student at East China University of Science and Technology and the University of Oregon in materials science and engineering. His research interests include electrocatalyst design and membrane-based electrolysis devices.

Liam P. Twight

Liam P. Twight received his B.S. in chemistry from California State University, Long Beach and is now a doctoral student in chemistry at the University of Oregon. He is studying the fundamental electrochemical aspects of the oxygen evolution reaction on transition metal oxides.

T. Nathan Stovall

T. Nathan Stovall is a third-year undergraduate student pursuing a B. S. in chemistry. His research at the University of Oregon is focused on developing novel OER catalysts for

PEMWE and studying the modes of degradation in AEMWE. After completion of his undergraduate studies, he plans to pursue a Ph.D. in chemistry investigating the fundamentals of renewable energy devices.

Acknowledgements. This work was funded by National Science Foundation grant 1955106 and DOE EERE grant DE-EE0008841.

References

1. Ayers, K.; Danilovic, N.; Ouimet, R.; Carmo, M.; Pivovar, B.; Bornstein, M. Perspectives on Low-Temperature Electrolysis and Potential for Renewable Hydrogen at Scale. *Annu. Rev. Chem. Biomol. Eng.* **2019,** *10* (1), 219-239.
2. Lindquist, G. A.; Xu, Q.; Oener, S. Z.; Boettcher, S. W. Membrane Electrolyzers for Impure-Water Splitting. *Joule* **2020,** *4* (12), 2549-2561.
3. Reier, T.; Nong, H. N.; Teschner, D.; Schlögl, R.; Strasser, P. Electrocatalytic Oxygen Evolution Reaction in Acidic Environments – Reaction Mechanisms and Catalysts. *Adv. Energy Mater.* **2017,** *7* (1), 1601275.
4. Cao, X.; Novitski, D.; Holdcroft, S. Visualization of Hydroxide Ion Formation upon Electrolytic Water Splitting in an Anion Exchange Membrane. *ACS Mater. Lett.* **2019,** *1* (3), 362-366.
5. Trasatti, S.; Petrii, O. A. Real Surface Area Measurements in Electrochemistry. *J. Electroanal. Chem.* **1992,** *327* (1), 353-376.
6. Matsumoto, Y.; Sato, E. Electrocatalytic Properties of Transition Metal Oxides for Oxygen Evolution Reaction. *Mater. Chem. Phys.* **1986,** *14* (5), 397-426.
7. Enman, L. J.; Stevens, M. B.; Dahan, M. H.; Nellist, M. R.; Toroker, M. C.; Boettcher, S. W. Operando X-ray Absorption Spectroscopy Shows Iron Oxidation is Concurrent with Oxygen Evolution in Cobalt-Iron (Oxy)hydroxide Electrocatalysts. *Angew. Chem. Int. Ed.* **2018,** *57*, 12840-12844.
8. Friebel, D.; Louie, M. W.; Bajdich, M.; Sanwald, K. E.; Cai, Y.; Wise, A. M.; Cheng, M.-J.; Sokaras, D.; Weng, T.-C.; Alonso-Mori, R.; Davis, R. C.; Bargar, J. R.; Nørskov, J. K.; Nilsson, A.; Bell, A. T. Identification of Highly Active Fe Sites in (Ni,Fe)OOH for Electrocatalytic Water Splitting. *J. Am. Chem. Soc.* **2015,** *137* (3), 1305-1313.
9. Görlin, M.; Chernev, P.; Ferreira de Araújo, J.; Reier, T.; Dresp, S.; Paul, B.; Krähnert, R.; Dau, H.; Strasser, P. Oxygen Evolution Reaction Dynamics, Faradaic Charge Efficiency, and the Active Metal Redox States of Ni–Fe Oxide Water Splitting Electrocatalysts. *J. Am. Chem. Soc.* **2016,** *138* (17), 5603-5614.
10. Li, N.; Bediako, D. K.; Hadt, R. G.; Hayes, D.; Kempa, T. J.; von Cube, F.; Bell, D. C.; Chen, L. X.; Nocera, D. G. Influence of Iron Doping on Tetravalent Nickel Content in Catalytic Oxygen Evolving Films. *Proc. Nat. Acad. Sci.* **2017,** *114* (7), 1486-1491.

11. Smith, R. D. L.; Pasquini, C.; Loos, S.; Chernev, P.; Klingan, K.; Kubella, P.; Mohammadi, M. R.; Gonzalez-Flores, D.; Dau, H. Spectroscopic Identification of Active Sites for the Oxygen Evolution Reaction on Iron-Cobalt Oxides. *Nat. Commun.* **2017,** *8* (1), 2022.
12. Gong, L.; Chng, X. Y. E.; Du, Y.; Xi, S.; Yeo, B. S. Enhanced Catalysis of the Electrochemical Oxygen Evolution Reaction by Iron(III) Ions Adsorbed on Amorphous Cobalt Oxide. *ACS Catal.* **2018,** *8* (2), 807-814.
13. Hunter, B. M.; Thompson, N. B.; Müller, A. M.; Rossman, G. R.; Hill, M. G.; Winkler, J. R.; Gray, H. B. Trapping an Iron(VI) Water-Splitting Intermediate in Nonaqueous Media. *Joule* **2018,** *2* (4), 747-763.
14. Chen, J. Y.; Dang, L.; Liang, H.; Bi, W.; Gerken, J. B.; Jin, S.; Alp, E. E.; Stahl, S. S. Operando Analysis of NiFe and Fe Oxyhydroxide Electrocatalysts for Water Oxidation: Detection of Fe^{4+} by Mossbauer Spectroscopy. *J. Am. Chem. Soc.* **2015,** *137* (48), 15090-15093.
15. Zhang, T.; Nellist, M. R.; Enman, L. J.; Xiang, J.; Boettcher, S. W. Modes of Fe Incorporation in Co-Fe (Oxy)hydroxide Oxygen Evolution Electrocatalysts. *ChemSusChem* **2019,** *12* (9), 2015-2021.
16. Trotochaud, L.; Ranney, J. K.; Williams, K. N.; Boettcher, S. W. Solution-Cast Metal Oxide Thin Film Electrocatalysts for Oxygen Evolution. *J. Am. Chem. Soc.* **2012,** *134* (41), 17253-17261.
17. Wu, J.; Ren, Z.; Du, S.; Kong, L.; Liu, B.; Xi, W.; Zhu, J.; Fu, H. A Highly Active Oxygen Evolution Electrocatalyst: Ultrathin CoNi Double Hydroxide/CoO Nanosheets Synthesized via Interface-Directed Assembly. *Nano Res.* **2016,** *9*, 713-725.
18. Stevens, M. B.; Enman, L. J.; Korkus, E. H.; Zaffran, J.; Trang, C. D. M.; Asbury, J.; Kast, M. G.; Toroker, M. C.; Boettcher, S. W. Ternary Ni-Co-Fe Oxyhydroxide Oxygen Evolution Catalysts: Intrinsic Activity Trends, Electrical Conductivity, and Electronic Band Structure. *Nano Res.* **2019,** *12*, 2288-2295.
19. Trotochaud, L.; Young, S. L.; Ranney, J. K.; Boettcher, S. W. Nickel-Iron Oxyhydroxide Oxygen-Evolution Electrocatalysts: the Role of Intentional and Incidental Iron Incorporation. *J. Am. Chem. Soc.* **2014,** *136* (18), 6744-6753.
20. Batchellor, A. S.; Kwon, G.; Laskowski, F. A. L.; Tiede, D. M.; Boettcher, S. W. Domain Structures of Ni and NiFe (Oxy)Hydroxide Oxygen-Evolution Catalysts from X-ray Pair Distribution Function Analysis. *J. Phys. Chem. C* . **2017,** *121* (45), 25421-25429.
21. Burke, M. S.; Kast, M. G.; Trotochaud, L.; Smith, A. M.; Boettcher, S. W. Cobalt-Iron (Oxy)hydroxide Oxygen Evolution Electrocatalysts: The Role of Structure and Composition on Activity, Stability, and Mechanism. *J. Am. Chem. Soc.* **2015,** *137* (10), 3638-3648.
22. Smith, A. M.; Trotochaud, L.; Burke, M. S.; Boettcher, S. W. Contributions to Activity Enhancement via Fe Incorporation in Ni-(Oxy)hydroxide/Borate Catalysts for Near-Neutral pH Oxygen Evolution. *Chem. Commun.* **2015,** *51* (25), 5261-5263.
23. Stevens, M. B.; Enman, L. J.; Batchellor, A. S.; Cosby, M. R.; Vise, A. E.; Trang, C. D. M.; Boettcher, S. W. Measurement Techniques for the Study of Thin Film Heterogeneous Water Oxidation Electrocatalysts. *Chem. Mater.* **2017,** *29* (1), 120-140.
24. Lee, S.; Banjac, K.; Lingenfelder, M.; Hu, X. Oxygen Isotope Labeling Experiments Reveal Different Reaction Sites for the Oxygen Evolution Reaction on Nickel and Nickel Iron Oxides. *Angew. Chem. Int. Ed.* **2019,** *58* (30), 10295-10299.
25. Roy, C.; Sebok, B.; Scott, S. B.; Fiordaliso, E. M.; Sørensen, J. E.; Bodin, A.; Trimarco, D. B.; Damsgaard, C. D.; Vesborg, P. C. K.; Hansen, O.; Stephens, I. E. L.; Kibsgaard, J.; Chorkendorff, I. Impact of Nanoparticle Size and Lattice Oxygen on Water Oxidation on $NiFeO_xH_y$. *Nat. Catal.* **2018,** *1* (11), 820-829.

26. Ferreira de Araújo, J.; Dionigi, F.; Merzdorf, T.; Oh, H.-S.; Strasser, P. Evidence of Mars-Van-Krevelen Mechanism in the Electrochemical Oxygen Evolution on Ni-Based Catalysts. *Angew. Chem. Int. Ed.* **2021,** 60, 2-10.
27. Moysiadou, A.; Lee, S.; Hsu, C.-S.; Chen, H. M.; Hu, X. Mechanism of Oxygen Evolution Catalyzed by Cobalt Oxyhydroxide: Cobalt Superoxide Species as a Key Intermediate and Dioxygen Release as a Rate-Determining Step. *J. Am. Chem. Soc.* **2020,** *142* (27), 11901-11914.
28. Zou, S.; Burke, M. S.; Kast, M. G.; Fan, J.; Danilovic, N.; Boettcher, S. W. Fe (Oxy)hydroxide Oxygen Evolution Reaction Electrocatalysis: Intrinsic Activity and the Roles of Electrical Conductivity, Substrate, and Dissolution. *Chem. Mater.* **2015,** *27* (23), 8011-8020.
29. Batchellor, A. S.; Boettcher, S. W. Pulse-Electrodeposited Ni–Fe (Oxy)hydroxide Oxygen Evolution Electrocatalysts with High Geometric and Intrinsic Activities at Large Mass Loadings. *ACS Catal.* **2015,** *5* (11), 6680-6689.
30. Burke, M. S.; Zou, S.; Enman, L. J.; Kellon, J. E.; Gabor, C. A.; Pledger, E.; Boettcher, S. W. Revised Oxygen Evolution Reaction Activity Trends for First-Row Transition-Metal (Oxy)hydroxides in Alkaline Media. *J. Phys. Chem. Lett.* **2015,** *6* (18), 3737-3742.
31. Enman, L. J.; Vise, A. E.; Burke Stevens, M.; Boettcher, S. W. Effects of Metal Electrode Support on the Catalytic Activity of Fe(oxy)hydroxide for the Oxygen Evolution Reaction in Alkaline Media. *ChemPhysChem* **2019,** *20* (22), 3089-3095.
32. Corrigan, D. A. The Catalysis of the Oxygen Evolution Reaction by Iron Impurities in Thin Film Nickel Oxide Electrodes. *J. Electrochem. Soc.* **1987,** *134* (2), 377-384.
33. Klaus, S.; Trotochaud, L.; Cheng, M.-J.; Head-Gordon, M.; Bell, A. T. Experimental and Computational Evidence of Highly Active Fe Impurity Sites on the Surface of Oxidized Au for the Electrocatalytic Oxidation of Water in Basic Media. *ChemElectroChem* **2016,** *3* (1), 66-73.
34. Haber, J. A.; Xiang, C.; Guevarra, D.; Jung, S.; Jin, J.; Gregoire, J. M. High-Throughput Mapping of the Electrochemical Properties of (Ni-Fe-Co-Ce)O_x Oxygen-Evolution Catalysts. *ChemElectroChem* **2014,** *1* (3), 524-528.
35. Louie, M. W.; Bell, A. T. An Investigation of Thin-Film Ni-Fe Oxide Catalysts for the Electrochemical Evolution of Oxygen. *J. Am. Chem. Soc.* **2013,** *135* (33), 12329-37.
36. Enman, L. J.; Burke, M. S.; Batchellor, A. S.; Boettcher, S. W. Effects of Intentionally Incorporated Metal Cations on the Oxygen Evolution Electrocatalytic Activity of Nickel (Oxy)hydroxide in Alkaline Media. *ACS Catal.* **2016,** *6* (4), 2416-2423.
37. Boettcher, S. W.; Surendranath, Y. Heterogeneous Electrocatalysis Goes Chemical. *Nat. Catal.* **2021,** *4* (1), 4-5.
38. Nong, H. N.; Falling, L. J.; Bergmann, A.; Klingenhof, M.; Tran, H. P.; Spöri, C.; Mom, R.; Timoshenko, J.; Zichittella, G.; Knop-Gericke, A.; Piccinin, S.; Pérez-Ramírez, J.; Cuenya, B. R.; Schlögl, R.; Strasser, P.; Teschner, D.; Jones, T. E. Key Role of Chemistry Versus Bias in Electrocatalytic Oxygen Evolution. *Nature* **2020,** *587* (7834), 408-413.
39. Stevens, M. B.; Trang, C. D. M.; Enman, L. J.; Deng, J.; Boettcher, S. W. Reactive Fe-Sites in Ni/Fe (Oxy)hydroxide Are Responsible for Exceptional Oxygen Electrocatalysis Activity. *J. Am. Chem. Soc.* **2017,** *139* (33), 11361-11364.
40. Subbaraman, R.; Tripkovic, D.; Chang, K. C.; Strmcnik, D.; Paulikas, A. P.; Hirunsit, P.; Chan, M.; Greeley, J.; Stamenkovic, V.; Markovic, N. M. Trends in Activity for the Water Electrolyser Reactions on 3d M(Ni,Co,Fe,Mn) Hydr(oxy)oxide Catalysts. *Nat. Mater.* **2012,** *11* (6), 550-557.
41. Ida, S.; Shiga, D.; Koinuma, M.; Matsumoto, Y. Synthesis of Hexagonal Nickel Hydroxide Nanosheets by Exfoliation of Layered Nickel Hydroxide Intercalated with Dodecyl Sulfate Ions. *J. Am. Chem. Soc.* **2008,** *130* (43), 14038-14039.

42. Deng, J.; Nellist, M. R.; Stevens, M. B.; Dette, C.; Wang, Y.; Boettcher, S. W. Morphology Dynamics of Single-Layered $Ni(OH)_2$/NiOOH Nanosheets and Subsequent Fe Incorporation Studied by *in Situ* Electrochemical Atomic Force Microscopy. *Nano Lett.* **2017,** *17* (11), 6922-6926.
43. Dette, C.; Hurst, M. R.; Deng, J.; Nellist, M. R.; Boettcher, S. W. Structural Evolution of Metal (Oxy)hydroxide Nanosheets during the Oxygen Evolution Reaction. *ACS Appl. Mater. Interfaces* **2019,** *11* (6), 5590-5594.
44. Chung, D. Y.; Lopes, P. P.; Farinazzo Bergamo Dias Martins, P.; He, H.; Kawaguchi, T.; Zapol, P.; You, H.; Tripkovic, D.; Strmcnik, D.; Zhu, Y.; Seifert, S.; Lee, S.; Stamenkovic, V. R.; Markovic, N. M. Dynamic Stability of Active Sites in Hydr(oxy)oxides for the Oxygen Evolution Reaction. *Nat. Energy* **2020,** *5* (3), 222-230.
45. Bates, M. K.; Qingying, J.; Doan, H.; Liang, W.; Mukerjee, S. Charge-Transfer Effects in Ni-Fe and Ni-Fe-Co Mixed-Metal Oxides for the Alkaline Oxygen Evolution Reaction. *ACS Catal.* **2016,** *6*, 155-161.
46. Dong, C.; Han, L.; Zhang, C.; Zhang, Z. Scalable Dealloying Route to Mesoporous Ternary CoNiFe Layered Double Hydroxides for Efficient Oxygen Evolution. *ACS Sustain. Chem. Eng.* **2018,** *6*, 16096-16104.
47. Xu, D.; Stevens, M. B.; Rui, Y.; DeLuca, G.; Boettcher, S. W.; Reichmanis, E.; Li, Y.; Zhang, Q.; Wang, H. The Role of Cr Doping in NiFe Oxide/(Oxy)hydroxide Electrocatalysts for Oxygen Evolution. *Electrochim. Acta* **2018,** *265*, 10-18.
48. Yang, Y.; Dang, L.; Shearer, M. J.; Sheng, H.; Li, W.; Chen, J.; Xiao, P.; Zhang, Y.; Hamers, R. J.; Jin, S. Highly Active Trimetallic NiFeCr Layered Double Hydroxide Electrocatalysts for Oxygen Evolution Reaction. *Adv. Energy Mater.* **2018,** *8* (15), 1703189.
49. Xu, D.; Stevens, M. B.; Cosby, M. R.; Oener, S. Z.; Smith, A. M.; Enman, L. J.; Ayers, K. E.; Capuano, C. B.; Renner, J. N.; Danilovic, N.; Li, Y.; Wang, H.; Zhang, Q.; Boettcher, S. W. Earth-Abundant Oxygen Electrocatalysts for Alkaline Anion-Exchange-Membrane Water Electrolysis: Effects of Catalyst Conductivity and Comparison with Performance in Three-Electrode Cells. *ACS Catal.* **2019,** *9* (1), 7-15.
50. Li, D.; Park, E. J.; Zhu, W.; Shi, Q.; Zhou, Y.; Tian, H.; Lin, Y.; Serov, A.; Zulevi, B.; Baca, E. D.; Fujimoto, C.; Chung, H. T.; Kim, Y. S. Highly Quaternized Polystyrene Ionomers for High Performance Anion Exchange Membrane Water Electrolysers. *Nat. Energy* **2020,** *5* (5), 378-385.
51. Lagadec, M. F.; Grimaud, A. Water Electrolysers with Closed and Open Electrochemical Systems. *Nat. Mater.* **2020,** *19* (11), 1140-1150.
52. Xiao, J.; Oliveira, A. M.; Wang, L.; Zhao, Y.; Wang, T.; Wang, J.; Setzler, B. P.; Yan, Y. Water-Fed Hydroxide Exchange Membrane Electrolyzer Enabled by a Fluoride-Incorporated Nickel–Iron Oxyhydroxide Oxygen Evolution Electrode. *ACS Catal.* **2021,** *11* (1), 264-270.
53. Xu, Q.; Oener, S. Z.; Lindquist, G.; Jiang, H.; Li, C.; Boettcher, S. W. Integrated Reference Electrodes in Anion-Exchange-Membrane Electrolyzers: Impact of Stainless-Steel Gas-Diffusion Layers and Internal Mechanical Pressure. *ACS Energy Lett.* **2020**, 305-312.
54. Lindquist, G. A.; Oener, S. Z.; Motz, A. A.; Keane, A.; Capuano, C.; Ayers, K. E.; Boettcher, S. W. Performance and durability of pure-water-fed anion-exchange-membrane electrolyzers using baseline materials and operation. *ACS Appl. Mater. Interfaces* **Submitted 2021**.
55. Soni, R.; Miyanishi, S.; Kuroki, H.; Yamaguchi, T. Pure Water Solid Alkaline Water Electrolyzer Using Fully Aromatic and High-Molecular-Weight Poly(fluorene-alt-tetrafluorophenylene)-trimethyl Ammonium Anion Exchange Membranes and Ionomers. *ACS Appl. Energy Mater.* **2021,** *4* (2), 1053-1058.

56. Carbone, A.; Zignani, S. C.; Gatto, I.; Trocino, S.; Aricò, A. S. Assessment of the FAA3-50 Polymer Electrolyte in Combination with a $NiMn_2O_4$ Anode Catalyst for Anion Exchange Membrane Water Electrolysis. *Int. J. Hydrog. Energy* **2020,** *45* (16), 9285-9292.
57. Faid, A. Y.; Xie, L.; Barnett, A. O.; Seland, F.; Kirk, D.; Sunde, S. Effect of Anion Exchange Ionomer Content on Electrode Performance in AEM Water Electrolysis. *Int. J. Hydrog. Energy* **2020,** *45* (53), 28272-28284.
58. Farhat, R.; Dhainy, J.; Halaoui, L. I. OER Catalysis at Activated and Codeposited NiFe-Oxo/Hydroxide Thin Films Is Due to Postdeposition Surface-Fe and Is Not Sustainable without Fe in Solution. *ACS Catal.* **2020,** *10* (1), 20-35.
59. Etzi Coller Pascuzzi, M.; Man, A. J. W.; Goryachev, A.; Hofmann, J. P.; Hensen, E. J. M. Investigation of the Stability of NiFe-(Oxy)hydroxide Anodes in Alkaline Water Electrolysis under Industrially Relevant Conditions. *Catal. Sci. Technol.* **2020,** *10* (16), 5593-5601.
60. Xie, L.; Kirk, D. W. Nickel Catalyst Migration in an Anion Exchange Membrane Fuel Cell. *Electrochim. Acta* **2020,** *364*, 137091.
61. Dresp, S.; Luo, F.; Schmack, R.; Kühl, S.; Gliech, M.; Strasser, P. An efficient Bifunctional Two-Component Catalyst for Oxygen Reduction and Oxygen Evolution in Reversible Fuel Cells, Electrolyzers and Rechargeable Air Electrodes. *Energy Environ. Sci.* **2016,** *9* (6), 2020-2024.
62. Hegge, F.; Lombeck, F.; Cruz Ortiz, E.; Bohn, L.; von Holst, M.; Kroschel, M.; Hübner, J.; Breitwieser, M.; Strasser, P.; Vierrath, S. Efficient and Stable Low Iridium Loaded Anodes for PEM Water Electrolysis Made Possible by Nanofiber Interlayers. *ACS Appl. Energy Mater.* **2020,** *3* (9), 8276-8284.
63. Maurya, S.; Lee, A. S.; Li, D.; Park, E. J.; Leonard, D. P.; Noh, S.; Bae, C.; Kim, Y. S. On the Origin of Permanent Performance Loss of Anion Exchange Membrane Fuel Cells: Electrochemical Oxidation of Phenyl Group. *J. Power Sources* **2019,** *436*, 226866.
64. Mondschein, J. S.; Callejas, J. F.; Read, C. G.; Chen, J. Y. C.; Holder, C. F.; Badding, C. K.; Schaak, R. E. Crystalline Cobalt Oxide Films for Sustained Electrocatalytic Oxygen Evolution under Strongly Acidic Conditions. *Chem. Mater.* **2017,** *29* (3), 950-957.
65. Wang, Z.; Zheng, Y.-R.; Chorkendorff, I.; Nørskov, J. K. Acid-Stable Oxides for Oxygen Electrocatalysis. *ACS Energy Lett.* **2020,** *5* (9), 2905-2908.
66. Jin, S. Are Metal Chalcogenides, Nitrides, and Phosphides Oxygen Evolution Catalysts or Bifunctional Catalysts? *ACS Energy Lett.* **2017,** *2* (8), 1937-1938.
67. Binninger, T.; Mohamed, R.; Waltar, K.; Fabbri, E.; Levecque, P.; Kotz, R.; Schmidt, T. J. Thermodynamic Explanation of the Universal Correlation between Oxygen Evolution Activity and Corrosion of Oxide Catalysts. *Nat. Sci. Rep.* **2015,** *5* (12167).
68. Suntivich, J.; May, K. J.; Gasteiger, H. A.; Goodenough, J. B.; Shao-Horn, Y. A Perovskite Oxide Optimized for Oxygen Evolution Catalysis from Molecular Orbital Principles. *Science* **2011,** *334*, 1383-1385.
69. May, K. J.; Carlton, C. E.; Stoerzinger, K. A.; Risch, M.; Suntivich, J.; Lee, Y.-L.; Grimaud, A.; Shao-Horn, Y. Influence of Oxygen Evolution during Water Oxidation on the Surface of Perovskite Oxide Catalysts. *J. Phys. Chem. Lett.* **2012,** *3*, 3264-3270.
70. Risch, M.; Grimaud, A.; May, K. J.; Stoerzinger, K. A.; Chen, T. J.; Mansour, A. N.; Shao-Horn, Y. Structural Changes of Cobalt-Based Perovskites upon Water Oxidation Investigate by EXAFS. *J. Phys. Chem. C.* **2013,** *117*, 8628 - 8635.
71. Baeumer, C.; Li, J.; Lu, Q.; Liang, A. Y.-L.; Jin, L.; Martins, H. P.; Duchon, T.; Glos, M.; Gericke, S. M.; Wohlgemuth, M. A.; Giesen, M.; Penn, E. E.; Dittmann, R.; Gunkel, F.; Waser, R.; Bajdich, M.; Nemsak, S.; Mefford, J. T.; Chueh, W. C. Tuning Electrochemically Driven Surface Transformations in Atomically Flat $LaNiO_3$ Thin Films for Water Electrolysis. *Nat. Mater.* **2021**, 20, 674-682.

72. Lopes, P. P.; Chung, D. Y.; Rui, X.; Zheng, H.; He, H.; Martins, P. F. B. D.; Strmcnik, D.; Stamenkovic, V. R.; Zapol, P.; Mitchell, J. F.; Klie, R. F.; Markovic, N. M. Dynamically Stable Active Sites from Surface Evolution of Perovskite Materials during the Oxygen Evolution Reaction. *J. Am. Chem. Soc.* **2021**, *143* (7), 2741-2750.

TOC Graphic